Modeling of quantum dot and nanoring pattern formation on pit-patterned semiconductor substrates

Materials Research Express

RECEIVED
7 June 2018

REVISED
2 July 2018

ACCEPTED FOR PUBLICATION
10 July 2018

PUBLISHED
18 July 2018

PAPER

Modeling of quantum dot and nanoring pattern formation on pit-patterned semiconductor substrates

Ashish Kumar , Lin Du and Dimitrios Maroudas

Department of Chemical Engineering, University of Massachusetts Amherst, Amherst, MA 01003-9303, United States of America

E-mail: maroudas@ecs.umass.edu

Keywords: quantum dots, nanorings, epitaxy, semiconductors, modeling and simulation

Supplementary material for this article is available online

Abstract

We develop a properly parameterized, three-dimensional continuum-scale kinetic model for monitoring the surface morphological evolution of coherently strained heteroepitaxial thin films that captures the morphological response of epitaxially grown Ge thin films on pit-patterned Si{100} substrates. The model accounts for curvature-driven atomic diffusion on the film surface, biaxial lattice misfit strain in the film, and the wetting potential between the film and the substrate. Self-consistent dynamical simulations based on our model show formation of complex nanostructures on the epitaxial film surface, including nanorings at the rims of pits, a single quantum dot at the center of a pit, as well as multiple quantum dots inside pits with rectangular openings, consistent with experimentally observed nanostructures. Our simulation results reproduce the variation in the formed nanostructural features observed experimentally by properly varying the key experimental parameters, namely, the pit size and the pit geometry. Our study sets the stage for designing systematic experimental protocols toward precise control of complex nanoring and quantum dot patterns forming on surfaces of epitaxially grown coherently strained semiconductor thin films.

1. Introduction

Because of their electronic confinement, semiconductor material nanostructures such as quantum dots and nanorings have a wide variety of applications in electronic and photonic devices [1–4], sensing [5, 6], and magnetic recording devices [7], among numerous others. One method of forming such nanostructures on surfaces of epitaxially grown semiconductor thin films is through Stranski-Krastanow (SK) growth [8, 9] due to biaxial misfit strain in the epitaxial film because of its lattice mismatch with the substrate. However, quantum dots formed as a result of SK growth instabilities nucleate randomly on the film surface and, typically, lack uniformity both in size and in their arrangement. This non-uniformity is usually undesirable for application purposes, where uniform positioning and ordering of nanostructures is required. To address this challenge of self-assembling uniformly arranged and consistently sized nanostructures in such epitaxially grown coherently strained thin films, recent studies have explored strategies for guiding nanostructure formation in epitaxial films by depositing them on substrates with a modified morphology [10–14].

Among various methods involving formation of self-assembled ordered quantum dots during epitaxial growth of thin films, a very successful one is that of growth of coherently strained thin films on pit-patterned substrate surfaces [15–18]. This method of formation of ordered nanostructures has been studied experimentally for various semiconductor heteroepitaxial film/substrate systems such as Ge/Si [15–17], InN/GaN [18], InAs/GaAs [19], and Ge/Si_3N_4 [20]. These experimental studies have reported nucleation of ordered nanostructures, such as periodic patterns of one or more quantum dots forming inside the pits [16, 17, 19] and nanoring-like structures forming at the rims of the pits [15, 16, 18, 20].

Many theoretical and computational studies using continuum-scale models and Monte Carlo simulations [21–25] have analyzed surface morphological evolution of epitaxial films grown on patterned substrates,

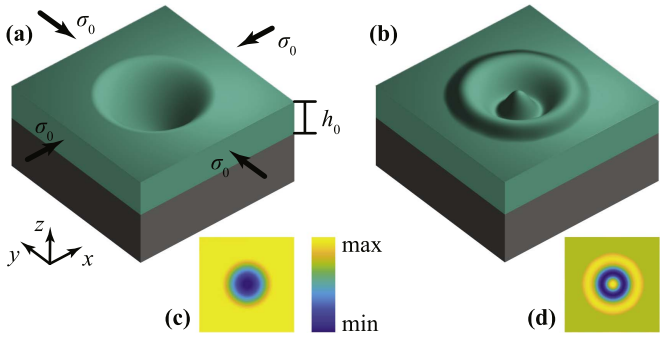

Figure 1. Schematic representation of the surface morphological transformation of a coherently strained thin film, deposited epitaxially on a pit-patterned substrate up to a nominal thickness h_0, from (a) its initial configuration consisting of a pit in the domain center mimicking the pit-patterned substrate to (b) a complex configuration with a nanoring forming at the rim of the pit and a quantum dot emerging from the center of the pit. 2D surface height contour maps of the configurations in (a) and (b) are shown in (c) and (d), respectively. In all cases, the unit cell is shown of a periodic pattern on the film surface.

including the formation of islands (quantum dots) on pit-patterned substrates. An analysis of film surface morphology based on a phase field model that characterized the resulting pit geometry on the surface of an epitaxial film on a pit-patterned substrate has been presented in [21]. Analysis of morphological stability and numerical simulations of morphological evolution of epitaxial film surfaces that have been perturbed according to plane-wave patterns have predicted asymptotic states of quantum dot patterns on the epitaxial film surface [22, 23]. Furthermore, analytical thermodynamic studies of strained island nucleation on patterned substrates [24], as well as Monte Carlo simulations of self-assembly and ordering mechanisms of Ge islands on pre-patterned Si{001} substrates [25] have been conducted. In spite of these elegant studies, formation of single and multiple quantum dots inside pits and of nanorings at pit rims on surfaces of epitaxial films on pit-patterned substrates has not been analyzed in detail or predicted in direct comparison with experimental findings.

In this article, we present a theoretical model for the surface evolution of coherently strained epitaxial thin films which are deposited on pit-patterned semiconductor substrates. The model predictions provide a comprehensive interpretation for the formation of the above mentioned interesting nanostructure patterns that have been observed in experiments. In our study, we emphasize on the diffusional kinetics of surface morphological evolution as well as on direct and systematic comparisons of our modeling predictions with detailed experimental observations of nanostructure pattern formation during Ge epitaxial growth on pit-patterned Si substrates. In our predictions and comparisons, we refer specifically to the Ge/Si heteroepitaxial system; however, our model can be parameterized for any heteroepitaxial film/substrate material system and used to develop growth strategies and guide the design of systematic experimental protocols toward precise control of ordered nanostructure patterns on epitaxial film surfaces.

2. Surface evolution model

We consider a coherently strained thin film grown epitaxially on a thick substrate, with a film surface morphology shown in figure 1(a) which mimics that of a film deposited through layer-by-layer growth on a pit-patterned substrate surface such as those in the experiments of [17]. Instead of performing a direct simulation of the growth of an epitaxial film from zero thickness to its final thickness h_0 as it happens in the experiments, we start with an initial configuration consisting of a thin film whose surface is at a distance h_0 above the surface of the substrate on which the film is deposited. This essentially means that the film's initial configuration, as shown in figure 1(a), takes the shape of the pit on the substrate surface with the pit repeated periodically, mimicking the substrate's pit pattern. In our study, we have examined two initial pit configurations, mimicking substrate surfaces with patterns of: (1) pits with a shape resembling an inverted truncated cone that has a circular pit opening; and (2) pits with a shape resembling an inverted truncated pyramid that has a rectangular or square pit opening. The wall of each pit is represented by half a wavelength of a cosinusoidal wave specified by a wave number k. At time $t = 0$, we let the film surface evolve according to our film surface evolution model detailed below. We find that over time the film surface with 'conical' pits as initial configuration evolves to form a complex nanopattern configuration with a nanoring forming at the rim of each pit as shown in figure 1(b). Together with this nanoring formation in the complex pattern, we predict that either one quantum dot or no quantum dot at all may form inside each pit depending on the lateral size of the pits, which we quantify through the diameter of the circular pit opening d_0. Moreover, we show that the number of quantum dots emerging from inside the pits in the final pattern also depends on the geometry of the initial pit configuration. If we start with a

'pyramidal' pit as an initial configuration as opposed to a 'conical' pit, we predict formation of a single quantum dot or multiple quantum dots depending on the lateral size of such a pyramidal pit with a rectangular opening.

The film is subject to an equibiaxial stress with nonzero stress components in the x- and y-directions of the Cartesian frame of reference of figure 1(a). The surface morphology of the film is parameterized with the surface height function $h(x, y, t)$. Using a Nernst-Einstein equation to express the surface atomic flux and the continuity equation to express mass conservation gives the height evolution equation

$$\frac{\partial h}{\partial t} = H'\nabla_s \cdot \left[\frac{\delta_s \Omega D_s}{k_B T} \cdot \nabla_s (U_E - \gamma_f \kappa + U_W)\right]. \tag{1}$$

In equation (1), $H' \equiv (1 + h_x^2 + h_y^2)^{1/2}$, $h_x \equiv \partial h/\partial x$ and $h_y \equiv \partial h/\partial y$, Ω is the atomic volume, δ_s / Ω is the number of surface atoms per unit area, k_B is the Boltzmann constant, T is temperature, D_s is the film surface atomic diffusivity, and ∇_s represents the surface gradient operator; within the bracketed flux expression in the right-hand side of equation (1), ∇_s acts on the chemical potential of the film surface atoms, which includes contributions from the densities of the elastic strain energy U_E, the surface energy $\gamma_f \kappa$, where κ is the surface curvature, and the wetting potential, U_W. The wetting potential density is given by

$$U_W = \frac{(\gamma_f - \gamma_s) b}{H' \pi (b^2 + h^2)} \tag{2}$$

according to the 'transition-layer' (of thickness b) model [26, 27], where γ_f and γ_s are the surface free energies per unit area of the film and substrate materials, respectively. For simplicity, we neglect both the surface diffusivity and the surface free energy anisotropies. U_E is computed by solving the elastostatic boundary-value problem (BVP) in the film and calculating the stress and strain tensors at every point on the film surface. As described in detail in [28], U_E is calculated asymptotically based on regular perturbation theory and keeping up to second-order terms in the asymptotic expansion. We should also mention that in the calculations of the elastic strain energy of the thin film, we use the bulk value of the elastic modulus of Ge for the thin film; although the elastic moduli of nanostructures can be quite different from the bulk material values, for a Ge/Si epitaxial system on a practically infinitely thick Si substrate and for the lattice mismatch between the film and substrate materials in this epitaxial system, we do not expect the elastic properties of Ge to be substantially different from their bulk values and cause any differences in the findings of this study. Dimensional analysis of equation (1) gives a length scale $l = M_s \gamma_f / \sigma_0^2$, where M_s is the biaxial modulus of the substrate [28] and σ_0 is the magnitude of the biaxial stress in the film in a reference-state configuration with planar film surface morphology, a time scale $\tau = k_B T l^4 / [\delta_s \Omega D_s \gamma_f]$, and a dimensionless parameter $\Xi_w = [2b(\gamma_s - \gamma_f) / (\pi h_0^3 \gamma_f)] l^2$ that expresses the strength of the wetting potential [28]. Using a Ge film on a Si substrate at 700 °C as a representative heteroepitaxial system, we estimate the values of l and τ as $l \approx 17$ nm and $\tau \approx 8.1$ min $\approx$485 s.

It should be mentioned that the governing equations and boundary-value problems in our model are the same with those of the model employed in [28]. However, the problems addressed in the two studies are different due to the different epitaxial film configurations involved. In [28], the film surface is merely perturbed from the perfectly planar morphology by a low-amplitude long-wavelength perturbation or a random perturbation (resembling thermal fluctuations), while here the surface of the film reflects the actual pit configuration of the patterned substrate as depicted in figure 1(a), i.e., the heteroepitaxial system geometries of the problems addressed in the two studies are substantially different. Also, importantly, in [28], the key geometrical parameter is the perturbation wavelength (for infinitesimally low amplitude), while here the pit size (diameter, depth, etc.) and overall geometry are important parameters as explained in the discussion of section 3. Finally, the analysis in [28] is relevant to film growth on substrates that, if patterned, the pattern consists of regular arrays of embedded quantum dots as opposed to the pit-patterned substrates examined here.

3. Simulation results and discussion

To explore the kinetics of the stressed film surface morphological evolution, we conduct systematic dynamical simulations according to the film evolution model of equation (1). In the simulations, we solve the elastostatic BVP self-consistently with the film surface propagation as described in [28] based on a spectral collocation method [27]; in this implementation, the film surface is discretized using 128 $\times$ 128 grid points and discrete fast Fourier transforms are performed. For the integration of equation (1), we employ an advanced operator splitting-based semi-implicit spectral method [29] with adaptive time step size. Using this implementation of our model, we carry out self-consistent dynamical simulations to explore the epitaxial film surface dynamics for the two geometries of initial configuration described above, namely, with pits resembling inverted truncated cones and pyramids. In the simulations, we start with a film thickness h_0 that is well above the critical film thickness required for SK morphological instability; for Ge/Si{100}, this critical thickness is $\approx$3 ML [8, 30, 31].

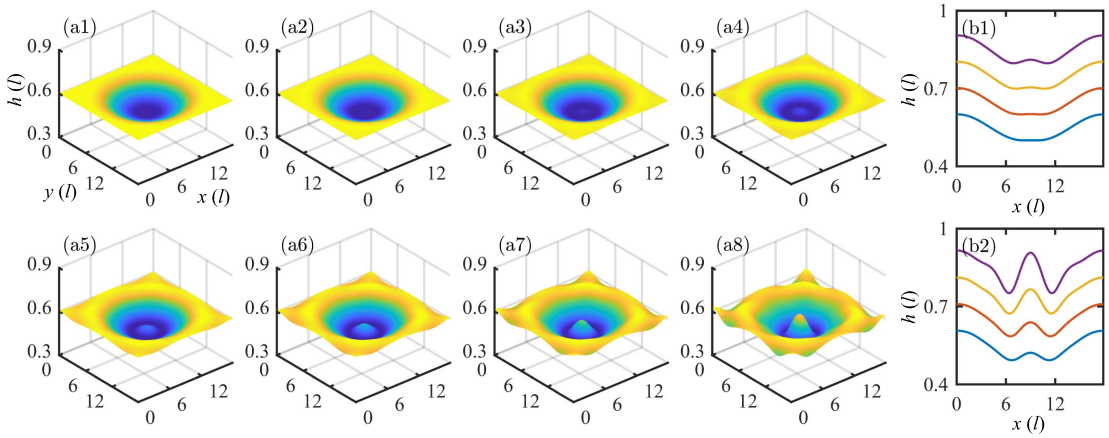

Figure 2. (a1-a8) Simulated evolving surface morphology, $h(x, y, t)$, of a coherently strained epitaxial film starting with an inverted truncated conical nanopit configuration with opening diameter of 17.7 l at (a1) $t = 0.0\ \tau$, (a2) $t = 0.3\ \tau$, (a3) $t = 0.6\ \tau$, (a4) $t = 0.9\ \tau$, (a5) $t = 1.2\ \tau$, (a6) $t = 1.5\ \tau$, (a7) $t = 1.8\ \tau$, and (a8) $t = 2.1\ \tau$. (b1, b2) 1D surface profiles, $h(x; y, t)$, along the x-direction and passing through the center of the unit cell of (a1)-(a4) and (a5)-(a8) are plotted in (b1) and (b2), respectively. In both (b1) and (b2), the surface profile evolution sequences are from the bottom to the top; in (b1/b2), the profiles of the configurations shown in (a1/a5), (a2/a6), (a3/a7), and (a4/a8) are colored blue, red, gold, and purple, respectively. In both (b1) and (b2), consecutive surface profiles have been displaced upwards (along the h-axis) by 0.1 l for clarity regarding their shapes. In all cases, a unit cell is shown of a periodic pattern on the film surface. Parameter values: $h_0 = 0.6\ l$, pit-pattern period $d_{\rm pit} = 18\ l$, pit depth =0.1 l, $k = 0.4\ l^{-1}$, and $\Xi_W = 0.0006$.

Figure 2 shows representative simulation results for the film surface morphological evolution according to our model for a film deposited on a substrate patterned with pits resembling inverted truncated cones. Figures 2(a1)–(a8) show 3D views of unit-cell configurations of a periodic pit pattern on the film surface as the surface evolves under the action of the driving forces of equation (1). In this case, the pit-pattern period, $d_{\rm pit}$, is 18 l. Our model predicts that starting with the initial configuration of figure 2(a1), the film surface evolves and leads to formation of a single quantum dot emerging from the center of the pit. This can be seen clearly from the evolving surface profiles along the x-axis through the center of the pit, which are shown in figures 2(b1) and (b2) for the configurations of figures 2(a1)–(a4) and figures 2(a5)–(a8), respectively. Our model also predicts the nucleation of a nanoring-like structure at the rim of the circular pit opening. It can be seen from the surface profiles in figures 2(b1) and (b2) that the pit deepens over time and the bottom-most part of the pit attains the critical film thickness. Our predictions are in good agreement with the experimental findings of [15–17] for epitaxial growth of Ge films on pit-patterned Si{100} substrates. A detailed direct comparison of our simulation results with the experimentally reported Ge film surface configurations is presented in the supplementary document is available online at stacks.iop.org/mrx/5/086303/mmedia. Specifically, in the supplementary document, detailed quantitative comparisons are presented between our simulation results and experimental findings reported in [17] in order to highlight that the simulations reproduce the nanostructures formed in the experiments and their main features.

Whether a quantum dot will form at the center of the pit or not depends on the initial opening diameter of the 'conical' pits. For example, for such conical pits with large opening diameters, as shown in figure 2(a1), a quantum dot forms at the center of the pit, whereas for conical pits with opening diameters smaller than a critical value quantum dot formation at the center of the pit is not predicted. A representative simulation result for a pit with a smaller-than-critical opening diameter (contrary to the pit depicted in figure 2) is shown in figures 3(a1)–(a5). Figures 3(a1)–(a4) show 2D contour maps of the evolving film surface shape within the unit cell of a periodic inverted truncated cone-shaped pit pattern with the initial configuration shown in figure 3(a1). Figure 3(a5) shows the surface profile of the initial configuration and the final configuration (depicted in figure 3(a4)) along the marked horizontal black solid line in the unit cell, indicating that, in this case, a quantum dot does not emerge from the center of the pit. Keeping all the other parameters fixed at their values that yielded the results of figure 2, we estimate from our simulations a critical conical pit opening diameter $d_{0,c} = 16.14\ l$ for quantum dot formation at the center of the pit. This estimation is based on the response diagram of figure 3(b), which shows the dependence of the height from the base of the pit, $h_{\rm QD}$, of quantum dots formed at the center of the pit in the final configuration as a function of the initial pit opening diameter.

The type of nanopattern formed on the evolving film surface also depends on the initial geometry of the pit in the pattern. To explore such pit geometry effects, we have analyzed the epitaxial film surface evolution in the case where the film is deposited on a substrate with a regular pattern of pits with a shape resembling that of an inverted truncated pyramid as opposed to an inverted truncated cone analyzed above. The pits shaped to resemble inverted truncated pyramids have rectangular (including square) openings. Evolution of epitaxial film

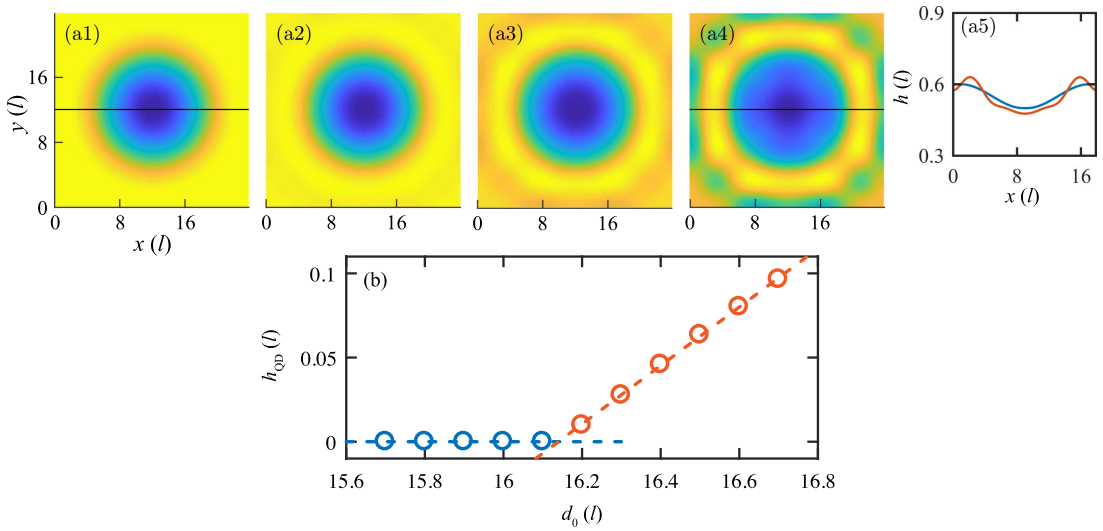

Figure 3. (a) 2D contour maps of simulated evolving surface morphology, $h(x, y, t)$, of a coherently strained thin film starting with a surface morphology that consists of a periodic arrangement of nanopits, with (a1) the top view of one such nanopit structure shown in the unit cell of the regular nanopit pattern for a conical pit with opening diameter of 16.0 l at (a1) $t = 0\ \tau$, (a2) $t = 0.7\ \tau$, (a3) $t = 1.5\ \tau$, and (a4) $t = 2.3\ \tau$. 1D surface profiles, $h(x; y, t)$, along the horizontal black solid lines marked on the 2D contour maps of (a1) and (a4) are plotted in blue and red, respectively, in (a5). (b) Height of quantum dots, h_{QD}, from the base of the pits at time $t = 2.3\ \tau$ as a function of the pit opening diameter d_0. The d_0 values that correspond to absence of quantum dots (h_{QD}=0) and formation of quantum dots at the center of the pit are denoted by blue and red open circles, respectively. In the simulations, $h_0 = 0.6\ l$, $d_{pit} = 18\ l$, pit depth =0.1 l, $k = 0.4\ l^{-1}$, and $\Xi_W = 0.0006$.

surfaces with such 'pyramidal' pits leads to formation of a nanoring-like structure at the rims of the pits similar to those observed in the previous class of 'conical' pits. However, we predict that for these 'pyramidal' pits, the number of the quantum dots formed within each pit depends on the length of the sides of the rectangular pit opening consistently with the experimental observations of [17]. Figures 4(a1)–(a4), (b1)–(b4), and (c1)–(c4) show 2D contour maps of the evolving film surface shape within the unit cell of a periodic inverted truncated pyramid-shaped pit pattern with the initial configuration shown in figures 4(a1), (b1), and (c1), respectively. In these initial configurations, the pit-opening perimeters increase such that the pit-opening widths (along the y-direction) for the initial configurations in figures 4(a1) and (b1) are equal, and the pit-opening lengths (along the x-direction) for the initial configurations in figures 4(b1) and (c1) also are equal. Figures 4(a4), (b4), and (c4) show the resulting patterns due to the evolution of the film surface mediated by diffusional (atomic transport) kinetics. It is clear from these results that the number of quantum dots that may form inside each pit [one, two, and four in the cases of figures 4(a4), (b4), and (c4), respectively] is strongly dependent on the size of the pit opening. In each case, the nanoring-like structure surrounding the pits in the final pattern is formed consistently at the rims of all the pits as can be seen from the surface profiles of figures 3(a5), 4(b5), and 4(c5). A systematic parametric study for determining the detailed quantum dot nanopatterns that form on surfaces of thin films grown epitaxially on pit-patterned substrates as a function of the precise pit geometry is beyond the scope of this article, but is currently underway and will be reported in a forthcoming publication.

4. Summary and conclusions

In summary, our theoretical model and dynamical simulations based on the model can capture the complex nanostructures and their patterns observed in experiments during epitaxial growth of Ge thin films on pit-patterned Si substrates. Our modeling results provide a fundamental kinetic interpretation of the experimental reports in the literature on quantum dot pattern formation on surfaces of epitaxial semiconductor films grown on pit-patterned semiconductor substrates. In addition to the parameters examined (i.e., varied) in this study, the pit wall slope is a parameter that plays an important role in the ensuing pattern formation on the epitaxial film surface: this parameter is captured through the wave number k in the pit geometry used here in the implementation of our model. In the case of pits resembling an inverted truncated cone, we have found that varying the pit wall slope, while keeping all other parameters constant, affects whether a quantum dot is formed at the center of the pit or not. A more systematic analysis of how parameters such as pit geometry, pit opening size, pit-pattern size (i.e., period), pit-wall slope, pit depth, and film thickness may be varied to determine the nanostructure pattern formation on epitaxial film surfaces will be presented in a subsequent publication. The present study, in conjunction with such future studies, can be used to guide the design of systematic

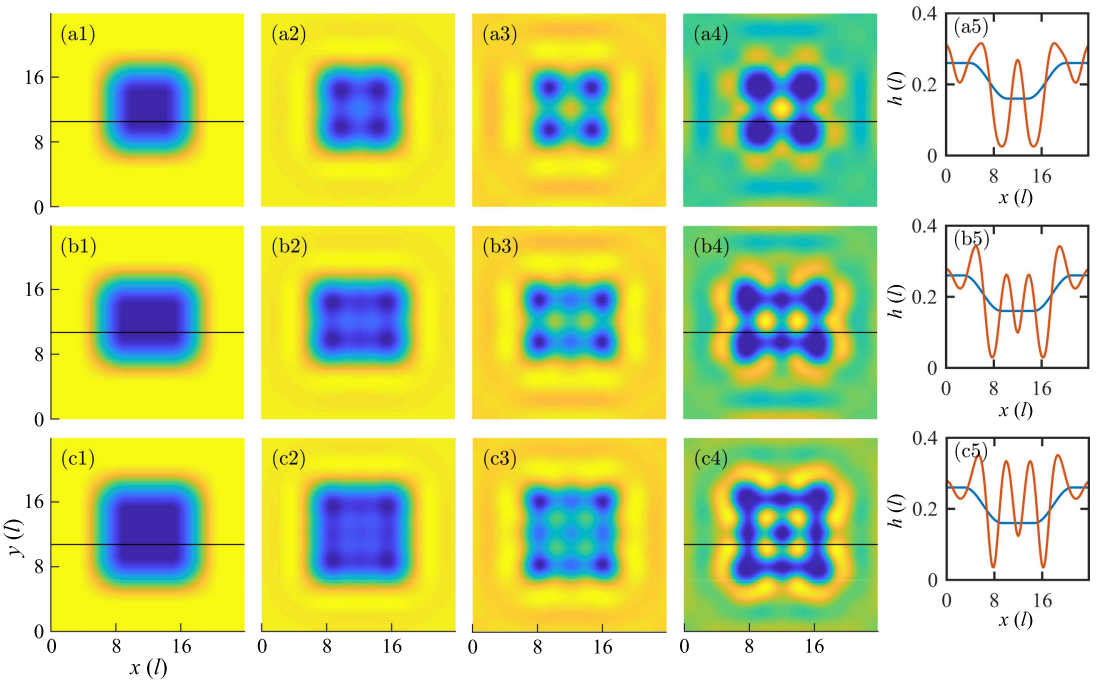

Figure 4. 2D contour maps of simulated evolving surface morphology, $h(x, y, t)$, of a coherently strained thin film starting with a surface morphology that consists of a periodic arrangement of nanopits, with (a1), (b1), and (c1) the top view of one such nanopit structure shown in the unit cell of the regular nanopit pattern for (a1-a5) a square pyramidal pit with equal opening length and width of 16.0 l at (a1) $t = 0\ \tau$, (a2) $t = 0.8\ \tau$, (a3) $t = 1.7\ \tau$, and (a4) $t = 2.6\ \tau$; (b1-b5) a rectangular pyramidal pit with opening length (along the x-axis) of 18.0 l and width (along the y-axis) of 16.0 l at (b1) $t = 0\ \tau$, (b2) $t = 0.8\ \tau$, (b3) $t = 1.7\ \tau$, and (b4) $t = 2.6\ \tau$; and (c1-c5) a square pyramidal pit with equal opening length and width of 18.0 l at (c1) $t = 0\ \tau$, (c2) $t = 0.8\ \tau$, (c3) $t = 1.7\ \tau$, and (c4) $t = 2.6\ \tau$. 1D surface profiles, $h(x; y, t)$, along the horizontal black solid lines marked on the 2D contour maps of (a1) and (a4), (b1) and (b4), and (c1) and (c4) are plotted in blue and red, respectively, in (a5), (b5), and (c5), respectively. In the simulations, $h_0 = 0.26\ l$, $d_{\rm pit} = 24\ l$, pit depth =0.1 l, $k = 0.5\ l^{-1}$, and $\Xi_W = 0.0072$.

experimental protocols for the discovery and precise control of nanostructure patterns forming on surfaces of epitaxially grown, coherently strained semiconductor thin films.

Acknowledgments

This work was supported by the US Department of Energy, Office of Basic Energy Sciences, Division of Materials Sciences and Engineering, under Award No. DE-FG02-07ER46407.

ORCID iDs

Ashish Kumar https://orcid.org/0000-0003-0085-2812
Dimitrios Maroudas https://orcid.org/0000-0001-9297-8839

References

[1] Yablonovitch E 1987 Inhibited spontaneous emission in solid-state physics and electronics *Phys. Rev. Lett.* **58** 2059–62
[2] O'Leary S K, Foutz B E, Shur M S and Eastman L F 2006 Potential performance of indium-nitride-based devices *Appl. Phys. Lett.* **88** 152113
[3] Xu G *et al* 2010 THz generation from InN films due to destructive interference between optical rectification and photocurrent surge *Semicond. Sci. Tech.* **25** 015004
[4] Metcalfe G D, Shen H, Wraback M, Koblmüller G, Gallinat C, Wu F and Speck J S 2010 Terahertz radiation from nonpolar InN due to drift in an intrinsic in-plane electric field *Appl. Phys. Express* **3** 092201
[5] Yue Z, Lisdat F, Parak W J, Hickey S G, Tu L, Sabir N, Dorfs D and Bigall N C 2013 Quantum-dot-based photoelectrochemical sensors for chemical and biological detection *ACS Appl. Mater. Inter.* **5** 2800–14
[6] Costa-Fernández J M, Pereiro R and Sanz-Medel A 2006 The use of luminescent quantum dots for optical sensing *TrAC-Trend Anal. Chem.* **25** 207–18
[7] Chou S Y, Wei M S, Krauss P R and Fischer P B 1994 Single-domain magnetic pillar array of 35 nm diameter and 65 Gbits/in.^{2} density for ultrahigh density quantum magnetic storage *J. Appl. Phys.* **76** 6673–5
[8] Eaglesham D J and Cerullo M 1990 Dislocation-free Stranski-Krastanow growth of Ge on Si(100) *Phys. Rev. Lett.* **64** 1943–6
[9] Ross F M, Tersoff J and Tromp R M 1998 Coarsening of self-assembled Ge quantum dots on Si(001) *Phys. Rev. Lett.* **80** 984–7

[10] Yakes M K, Cress C D, Tischler J G and Bracker A S 2010 Three-dimensional control of self-assembled quantum dot configurations *ACS Nano* **4** 3877–82
[11] Lee J, Wang Z M, Strom N, Mazur Y I and Salamo G 2006 InGaAs quantum dot molecules around self-assembled GaAs nanomound templates *Appl. Phys. Lett.* **89** 202101
[12] Wong P S, Balakrishnan G, Nuntawong N, Tatebayashi J and Huffaker D L 2007 Controlled InAs quantum dot nucleation on faceted nanopatterned pyramids *Appl. Phys. Lett.* **90** 183103
[13] Schmidt O G, Deneke C, Kiravittaya S, Songmuang R, Heidemeyer H, Nakamura Y, Zapf-Gottwick R, Muller C and Jin-Phillipp N Y 2002 Self-assembled nanoholes, lateral quantum-dot molecules, and rolled-up nanotubes *IEEE J. Sel. Top. Quant.* **8** 1025–34
[14] Wang L *et al* 2008 Towards deterministically controlled InGaAs/GaAs lateral quantum dot molecules *New J. Phys.* **10** 045010
[15] Grydlik M, Brehm M and Schäffler F 2012 Morphological evolution of Ge/Si(001) quantum dot rings formed at the rim of wet-etched pits *Nanoscale Res. Lett.* **7** 601
[16] Brehm M, Grydlik M, Tayagaki T, Langer G, Schäffler F and Schmidt O G 2015 Photoluminescence investigation of strictly ordered Ge dots grown on pit-patterned Si substrates *Nanotechnology* **26** 225202
[17] Grydlik M, Langer G, Fromherz T, Schäffler F and Brehm M 2013 Recipes for the fabrication of strictly ordered Ge islands on pit-patterned Si(001) substrates *Nanotechnology* **24** 105601
[18] Kuo C-T, Hsu L-H, Lai Y-Y, Cheng S-Y, Kuo H-C, Lin C-C and Cheng Y-J 2017 Site-controlled crystalline InN growth from the V-pits of a GaN substrate *Appl. Surf. Sci.* **405** 449–54
[19] Kiravittaya S, Rastelli A and Schmidt O G 2009 Advanced quantum dot configurations *Rep. Prog. Phys.* **72** 046502
[20] Sarkar S S, Katiyar A K, Sarkar A, Dhar A, Rudra A, Khatri R K and Ray S K 2018 Germanium growth on electron beam lithography patterned Si_3N_4/Si(001) substrate using molecular beam epitaxy *Appl. Surf. Sci.* **437** 144–51
[21] Salvalaglio M, Backofen R, Voigt A and Montalenti F 2017 Morphological evolution of pit-patterned Si(001) substrates driven by surface-energy reduction *Nanoscale Research Letters* **12** 554
[22] Aqua J-N and Xu X 2015 Growth of quantum dots on pit-patterns *Surf. Sci.* **639** 20–4
[23] Aqua J-N and Xu X 2014 Directed self-organization of quantum dots *Phys. Rev.* E **90** 030402
[24] Hu H, Gao H J and Liu F 2008 Theory of directed nucleation of strained islands on patterned substrates *Phys. Rev. Lett.* **101** 216102
[25] Pascale A, Berbezier I, Ronda A and Kelires P C 2008 Self-assembly and ordering mechanisms of Ge islands on prepatterned Si(001) *Phys. Rev.* B **77** 075311
[26] Spencer B J 1999 Asymptotic derivation of the glued-wetting-layer model and contact-angle condition for Stranski-Krastanow islands *Phys. Rev.* B **59** 2011–7
[27] Pang Y and Huang R 2006 Nonlinear effect of stress and wetting on surface evolution of epitaxial thin films *Phys. Rev.* B **74** 075413
[28] Du L and Maroudas D 2016 Theory of multiple quantum dot formation in strained-layer heteroepitaxy *Appl. Phys. Lett.* **109** 023103
[29] Tegze G, Bansel G, Tóth G I, Pusztai T, Fan Z and Gránásy L 2009 Advanced operator splitting-based semi-implicit spectral method to solve the binary phase-field crystal equations with variable coefficients *J. Comp. Phys.* **228** 1612–23
[30] LeGoues F K, Copel M and Tromp R 1989 Novel strain-induced defect in thin molecular-beam epitaxy layers *Phys. Rev. Lett.* **63** 1826–9
[31] Williams A A, Thornton J M C, Macdonald J E, van Silfhout R G, van der Veen J F, Finney M S, Johnson A D and Norris C 1991 Strain relaxation during the initial stages of growth in Ge/Si(001) *Phys. Rev.* B **43** 5001–11